PERGAMON

Solid-State Electronics 45 (2001) 193–197

SOLID-STATE ELECTRONICS

Technical Note

# A physically-based semi-empirical effective mobility model for MOSFET compact $I$–$V$ modeling

K.Y. Lim, X. Zhou *

*School of Electrical and Electronic Engineering, Nanyang Technological University, Singapore 639798, Singapore*

Received 25 November 1999; received in revised form 3 August 2000

**Abstract**

A physically-based effective mobility model is presented, which includes Coulombic, phonon, and surface roughness scattering mechanisms. The model is semi-empirical and consists of three physics-based fitting parameters to be extracted with a single measurement of terminal current. The developed model is shown to be more physical than the commonly-used empirical model, and the doping dependence can be modeled after parameter extraction. The model has been verified with excellent prediction to the experimental data with broad bias and doping variations. © 2001 Published by Elsevier Science Ltd. All rights reserved.

*Keywords:* Effective mobility; MOSFET; Compact model

## 1. Introduction

Carrier mobility is one of the most important parameters in modeling the current–voltage ($I$–$V$) characteristics of modern MOSFET's. Accurate mobility models require incorporation of all the basic scattering mechanisms in the inversion layer. At least three important scattering mechanisms have been identified, namely, Coulombic scattering, phonon scattering, and surface roughness scattering. Microscopically, mobility is a measure of the individual scattering mechanisms. Physically-based mobility models for numerical simulation [1] treat scattering in momentum space macroscopically, with local field and doping variations in real space. However, they are too complicated for use in circuit simulation. Most mobility models for circuit simulation are semi-empirical in nature, with fitting parameters to relate the model to the measured terminal $I$–$V$ characteristics. There is always a tradeoff between the physics to be included from first-principle calculations and the computational efficiency as well as ease of parameter extraction.

In this note, a simplified effective mobility model based on the well-known Matthiessen's summation of the above-mentioned scattering mechanisms is presented. The model is formulated based on results from well-known first-principle theory but with a simple one-step parameter extraction. The compact model maintains the physical form and allows prediction of MOSFET current with different bias and doping conditions.

## 2. Effective mobility model

For compact mobility modeling, it is well known that the effective mobility is solely a function of the effective transverse field [2]

$$E_{\text{eff}} = \frac{Q_{\text{B}} + \eta Q_{\text{inv}}}{\varepsilon_{\text{Si}}} = \frac{1}{6t_{\text{ox}}}\left(V_{\text{gs}} + V_{\text{t}}\right), \tag{1}$$

where it is assumed that the channel inversion charge is proportional to the gate overdrive [$Q_{\text{inv}} = C_{\text{ox}}(V_{\text{gs}} - V_{\text{t}})$] and the depletion charge is proportional to the threshold voltage ($Q_{\text{B}} \approx C_{\text{ox}} V_{\text{t}}$). $\eta$ in Eq. (1) is 1/2 for $\langle 100 \rangle$ electrons [2]. Eq. (1) conveniently relates the effective

* Corresponding author. Tel.: +65-790-4532; fax: +65-791-2687.

*E-mail address:* exzhou@ntu.edu.sg (X. Zhou).


PII: S0038-1101(00)00190-8

field to the terminal voltage and device parameters ($V_t$ and $t_{ox}$), and is valid as long as $V_{gs} > V_t$.

Our effective mobility model is formulated based on the universal mobility curve (UMC) with three scattering mechanisms: Coulombic, $\mu_{co}$, phonon, $\mu_{ph}$, and surface roughness, $\mu_{sr}$, scatterings. Two assumptions are introduced to simplify the model. First, at room temperature and high field, Coulombic mobility can be assumed as a constant:

$$\mu_{co} = \mu_1 \tag{2}$$

since inherently Coulombic scattering is not a function of the electric field [3], but a function of doping (unscreened) and electron (screened) densities. Secondly, the mobility due to 2-D phonon scattering is based on [3,4]:

$$\mu_{ph} = \frac{A}{E_{eff}} + \frac{BN^{\gamma_m}}{TE_{eff}^{1/3}} \approx \frac{BN^{\gamma_m}}{TE_{eff}^{1/3}} = \frac{\mu_2}{E_{eff}^{1/3}}, \tag{3}$$

and we assume that, at high field, the first term $(A/E_{eff})$ can be ignored since the inversion layer thickness is dominated by the (1/3)-power dependence [3], which is the electrical quantum limit when all channel electrons lie in the lowest quantized subband [5]. It will be shown in Section 3 that these two assumptions are satisfied in the region where the two parameters ($\mu_1$ and $\mu_2$) are extracted. The mobility due to surface roughness scattering is adopted from [3]:

$$\mu_{sr} = \frac{CN^{\gamma_m}}{E_{eff}^2} = \frac{\mu_3}{E_{eff}^2}. \tag{4}$$

Then, based on Matthiessen's summation rule, it can be shown (with some algebra) that the total effective mobility is given by

$$\mu_{eff} = \left(\frac{1}{\mu_{co}} + \frac{1}{\mu_{ph}} + \frac{1}{\mu_{sr}}\right)^{-1} = \frac{\mu_1}{1 + (\mu_1/\mu_2)E_{eff}^{1/3} + (\mu_1/\mu_3)E_{eff}^2}, \tag{5a}$$

where

$$\mu_2 = BN^{\gamma_m}/T, \tag{5b}$$

$$\mu_3 = CN^{\gamma_m}. \tag{5c}$$

$\mu_1$, $\mu_2$, and $\mu_3$ have definite physical meanings. However, to relate the compact $\mu_{eff}$ model to the measured $I_{ds}$ data, they are used as empirical fitting parameters. If $\gamma_m$ is zero, extracting $\mu_2$ and $\mu_3$ is equivalent to extraction of $B/T$ and $C$.

This model has a similar form as the popular empirical universal mobility model:

$$\mu_{umc} = \frac{\mu_0}{1 + (E_{eff}/E_{crit})^{\theta}} \tag{6}$$

with $\mu_0$, $E_{crit}$, and $\theta$ as fitting parameters. The improvement of our new model is that it preserves the correct power-law dependency resulting from first-principle calculations and, as will be shown in Section 3, it allows doping dependence to be modeled based on the physically-derived expressions.

## 3. Parameter extraction and model prediction

Since mobility is not a function of the channel length, $\mu_1$, $\mu_2$, and $\mu_3$ can be extracted from long-channel $I$–$V$ data using the Levenberg–Marquardt non-linear least-square technique. Our long-channel $I_{ds}$ model is

$$I_{ds} = \mu_{eff} C_{ox} \frac{W}{L_{eff}} \left[ (V_{gs} - V_t) V_{ds} - \frac{A_b}{2} V_{ds}^2 \right] \tag{7a}$$

in linear region and

$$I_{ds} = v_{sat} W C_{ox} \frac{(V_{gs} - V_t)^2}{V_{gs} - V_t + A_b E_{sat} L_{eff}} \tag{7b}$$

in saturation region, where

$$A_b = 1 + \zeta \frac{\gamma}{2\sqrt{2\phi_B - V_{bs}}} \tag{7c}$$

is the bulk-charge factor [6], with an empirical fitting parameter $\zeta$.

$$\gamma = \frac{\sqrt{2q\varepsilon_{Si}N_{ch}}}{C_{ox}} \tag{7d}$$

is the body-effect parameter.

$$\phi_B = \frac{kT}{q} \ln\left(\frac{N_{ch}}{n_i}\right) \tag{7e}$$

is the bulk Fermi potential. The threshold voltage is based on the "critical-current at linear-threshold" definition [7] and is modeled by

$$V_t = V_{FB} + 2\phi_B + \gamma\sqrt{2\phi_B - V_{bs}} \tag{8}$$

for long-channel devices, where $V_{FB}$ is the flat-band voltage.

The measured $I_{ds}$ and $V_t$ data for this work are from 0.25 μm CMOS wafers with drawn gate length of 10 μm and width of 20 μm ($t_{ox}$ is 59 Å). The effective channel doping, $N_{ch}$, in the $V_t$ equation is first extracted from the measured $V_t$–$V_{bs}$ data (wafer #15) [8]. Then, a one-step non-linear regression on Eq. (7a) is performed using the linear $I_{ds}$–$V_{gs}$ data ($V_{ds} = 0.1$ V, $V_{gs} > V_t$, and setting $\zeta = 1$) to extract $\mu_1$, $\mu_2$, and $\mu_3$, as shown in Fig. 1 (solid symbol). This condition for parameter extraction justifies the two assumptions made in the mobility formulation. For $t_{ox} \sim 59$ Å, $V_t \sim 0.55$ V, and $V_t < V_{gs} < 2.5$ V, $E_{eff}$ is in the range of 0.3–0.9 MV cm$^{-1}$, which is in the region of the experimental $\mu_{eff}$–$E_{eff}$ curve [9] in which the (1/3)-power and square-law dependence is dominant. At

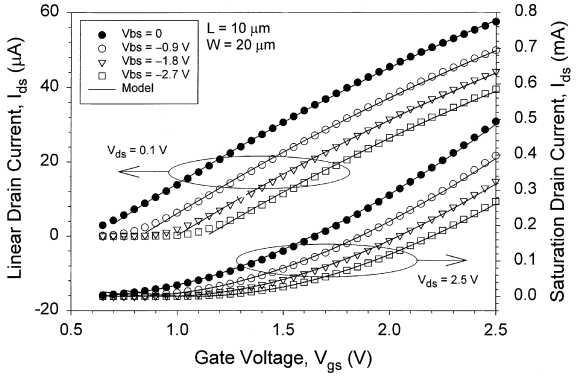


Fig. 1. Measured (symbols) and modeled (lines) linear and saturation $I_{ds}$–$V_{gs}$ characteristics, with data in solid symbols used for parameter extraction. Model prediction to data with different body bias is shown by the open symbols.

10-μm gate length, series resistance and channel-length modulation effects can also be ignored. After mobility-parameter extraction, $\zeta$ is extracted by fitting Eq. (7b) to the saturation $I_{ds}$–$V_{gs}$ data ($V_{ds} = 2.5$ V, $V_{gs} > V_t$), as also shown in Fig. 1.

Once the mobility parameters are extracted, excellent predictions of the model to the measured $I_{ds}$–$V_{gs}$ and $I_{ds}$–$V_{ds}$ characteristics at various $V_{bs}$ and $V_{gs}$ conditions are demonstrated, as shown in Figs. 1 and 2, respectively. The unified $I_{ds}$ model is given by

$$I_{ds} = \frac{\mu_{eff} C_{ox}}{1 + V_{deff}/(E_{sat} L_{eff})} \times \frac{W}{L_{eff}} \left[ (V_{gs} - V_t) V_{deff} - \frac{A_b}{2} V_{deff}^2 \right], \quad (9)$$

where $V_{deff}$ is the saturation voltage with a smoothing function used in BSIM3v3 [10]:

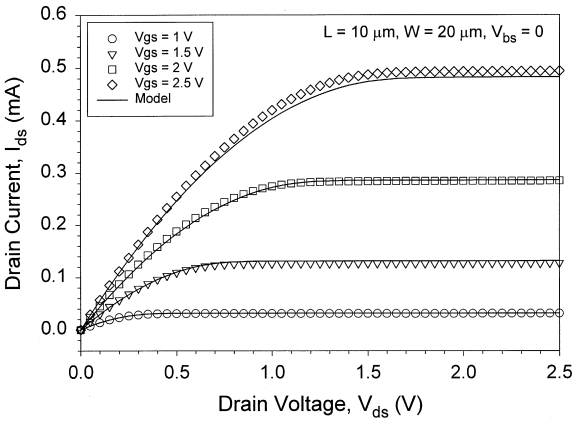


Fig. 2. Prediction of the unified $I_{ds}$ model (lines) to the measured (symbols) $I_{ds}$–$V_{ds}$ characteristics.

$$V_{deff} = V_{dsat} - 1/2 \left[ V_{dsat} - V_{ds} - \delta_s + \sqrt{(V_{dsat} - V_{ds} - \delta_s)^2 + 4\delta_s V_{dsat}} \right]. \quad (10)$$

Unlike BSIM3v3 [10], our mobility model has no explicit body-bias dependence, which has been accurately modeled by the threshold voltage [8].

The three parameters thus extracted physically represent the "weighted average" of the three scattering mechanisms in the respective regions of their contribution for the range of the gate bias (0.6–2.5 V) from the actual measured device (of course, within the validity of the $I_{ds}$ and $V_t$ models). When the modeled $\mu_{eff}$–$E_{eff}$ curve is plotted on a log–log scale in Fig. 3 (solid line), it shows the three-slope regions (0, $-1/3$ and $-2$), as indicated. As illustrated by the dashed lines, the "composite" $\mu_{eff}$ follows the asymptotes when surface scattering is ignored ($\mu_3 = \infty$) at low field and phonon scattering is ignored ($\mu_2 = \infty$) at high field. As can be seen, $\mu_1$ represents the low-field ($E_{eff} \to 0$) mobility due to the unscreened Coulombic scattering. At high field, since $\mu_{ph}$ and $\mu_{sr}$ are dominant, the error due to the assumption of $E_{eff}$-independent $\mu_{co}$ should be small.

On the other hand, when the empirical UMC model (6) is extracted from the same $I_{ds}$–$V_{gs}$ data and plotted in Fig. 3 (dotted line), although it fits the $I$–$V$ data equally well, the $\mu_{eff}$–$E_{eff}$ behavior is obviously not as physical as our model. With the extracted $E_{crit} = 1.5$ MV cm$^{-1}$ and $\theta = 2.8$, $(1/E_{crit})^{\theta} = 0.317$, which is close to $(\mu_1/\mu_3) = 0.33$ for the $\mu_{sr}$ term in our model. However, because of the missing $1/E_{eff}^{1/3}$ term, $\theta$ in the UMC model becomes larger than 2 and $\mu_0$ is "forced" to have a smaller value, which are all less physical.

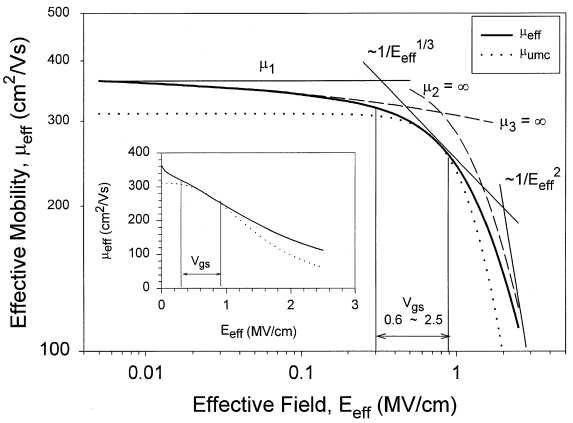


Fig. 3. Behavior of the extracted $\log(\mu_{eff})$–$\log(E_{eff})$ curve (—) compared to that of the UMC model extracted from the same $I_{ds}$–$V_{gs}$ data in the $V_{gs}$ range indicated. The same curves on linear–linear scale are shown in the inset. Asymptotes of the same $\mu_{eff}$ model with $\mu_2 = \infty$ and $\mu_3 = \infty$ are shown in dashed lines.

In Eqs. (3) and (4), the channel-doping term, $N^{\gamma_m}$, was introduced to fit the non-local UMC to the mobility model derived from local-field formulation [3]. Different values of $B$, $C$, and $\gamma_m$ have been adopted in different semi-empirical models or first-principle calculations [1,3]. In our formulation, without a priori knowledge of $\gamma_m$, we first indirectly determine $\mu_1$, $\mu_2$, and $\mu_3$ from the terminal $I$–$V$ data. Then, from Eqs. (5b) and (5c), and assuming a value for $\gamma_m$, the empirical fitting parameters $B$ and $C$ can be calculated. At a new doping $N'$, the doping-dependent mobility can be obtained from

$$\mu_2' = \left(N'/N\right)^{\gamma_m} \mu_2, \tag{11a}$$

$$\mu_3' = \left(N'/N\right)^{\gamma_m} \mu_3, \tag{11b}$$

in which $\mu_2$ and $\mu_3$ are extracted (calibrated) at doping $N$ (wafer #15). The doping-dependent mobility modeling with our proposed model is investigated and illustrated with the following example.

Experimental threshold voltages and saturation currents ($I_{dsat}$ at $V_{gs} = V_{ds} = 2.5$V) are obtained from the same wafer split-lot (wafers #17, #18, and #19) with changes only in $V_t$-adjustment implant dose. An empirical relationship between the channel doping, $N_{ch}$, and implant dose, $\Phi$, has been found [8,11] by fitting the $V_t$ model (8) to the measured $V_t$–$V_{bs}$ data:

$$N_{ch} = 1.426 \times 10^{17} + 7.231 \times 10^4 \Phi \ (\mathrm{cm}^{-3}), \tag{12}$$

where $\Phi$ is in $\mathrm{cm}^{-2}$. The modeled $V_t$–$\Phi$ curve is shown in Fig. 4 (open symbol). If the parameter set ($\mu_1$, $\mu_2$, $\mu_3$) extracted from wafer #15 is extended to other wafers for $I_{dsat}$ prediction (i.e., no doping dependence, or $\gamma_m = 0$), the average relative error, defined as

$$\langle \mathrm{Err} \rangle = \frac{1}{n} \sum_{i=1}^{n} \left\{ \frac{\left| I^{(i)}_{\text{dsat-measured}} - I^{(i)}_{\text{dsat-modeled}} \right|}{I^{(i)}_{\text{dsat-measured}}} \right\} \times 100\% \tag{13}$$

($n = 4$ for the four wafers), is found to be ~0.93%. The predicted $I_{dsat}$ is shown in Fig. 4 (solid line). If, however, we model the doping dependence of $\mu_2$ and $\mu_3$ through Eqs. (11a) and (11b) (using Eq. (12) for $N'$) for different values of $\gamma_m$ (ranging from 0 to 0.2), the doping dependence of $I_{dsat}$ (through $\mu_2'$ and $\mu_3'$) can be modeled semi-empirically. And, it is found that when $\gamma_m > 0.035$, the error in $I_{dsat}$ starts to increase (as shown in the inset of Fig. 4). The modeled $I_{dsat}$–$\Phi$ curve for $\gamma_m = 0.035$ (with minimum error of ~0.91%) is shown in Fig. 4 by the dotted line. This verifies the postulation [3] that $\gamma_m$ should theoretically be zero, and a non-zero $\gamma_m$ is only needed to account for the non-local field approximation in a local-mobility formulation. Our approach to modeling the doping-dependent mobility semi-empirically has demonstrated the tradeoff between ease of parameter extraction and physical fitting to measurement data.

## 4. Conclusions

In conclusion, a semi-empirical mobility model based on first-principle calculation has been formulated and verified with prediction of experimental data for various bias and doping conditions. The model includes basic scattering mechanisms and doping dependence, and yet, retains the compact form for easy parameter extraction and drain-current modeling. This model (with the same parameters) has been successfully applied to a complete

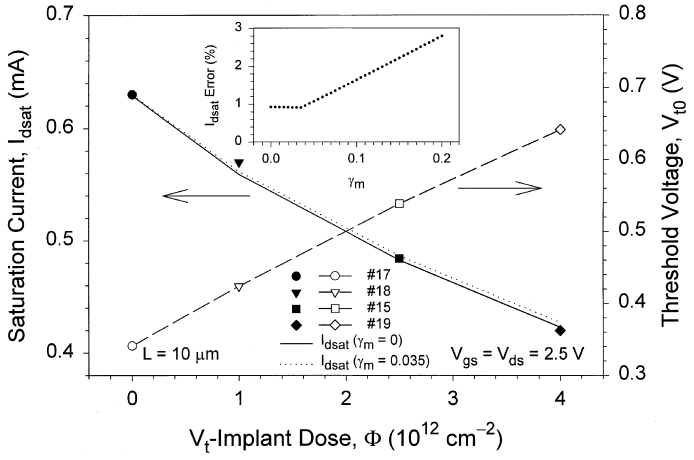


Fig. 4. Measured saturation current (solid symbols) and modeled threshold voltage (open symbols) from the four wafers with different $V_t$-implant dose. The average relative error in $I_{dsat}$ versus $\gamma_m$ is shown in the inset. The modeled $I_{dsat}$ with $\gamma_m = 0$ and 0.035 are shown by the solid and dotted lines, respectively.

$I_{ds}$ modeling of the short-channel devices (down to 0.2 μm) on the same wafer [12].

## Acknowledgements

Chartered Semiconductor Manufacturing Ltd. for providing the experimental data for this work is gratefully acknowledged.

## References

[1] Lombardi C, Manzizni S, Saporito A, Vanzi M. IEEE Trans Comput Aid Des 1988;CAD-7:1164–71.
[2] Sabnis AG, Clemens JT. IEDM Tech Dig 1979:18–21.
[3] Mujtaba SA. PhD Thesis, Stanford University, 1995.
[4] Mujtaba SA, Pinto MR, Boulin DM, Rafferty CS, Dutton RW. Proc SISDEP'95, Erlangen, Germany, 1995: 424–7.
[5] Villa S, Lacaita AL, Perron LM, Bez R. IEEE Trans Electron Dev 1998;45:110–5.
[6] Tsividis YP. Operation and modeling of the MOS transistor. New York: McGraw-Hill; 1987.
[7] Zhou X, Lim KY, Lim D. IEEE Trans Electron Dev 1999;46:807–9.
[8] Zhou X, Lim KY, Lim D. IEEE Trans Electron Dev 2000;47:214–21.
[9] Takagi S, Iwase M, Toriumi A. IEDM Tech Dig 1988:398–401.
[10] Cheng Y, Chan M, Hui K, Jeng MC, Liu Z, Huang J, Chen K, Chen J, Tu R, Ko PK, Hu C. BSIM3v3 manual. UC Berkeley, CA, 1996.
[11] Lim KY, Zhou X, Lim D. Proc MSM99. Puerto Rico, 1999: 423–6.
[12] Zhou X, Lim KY, revised and submitted to IEEE Trans Electron Dev.